Discovering Novel Inorganic Superionic Conductors with High-Throughput Virtual Screening Enhanced by Graph Neural Networks and Generative Models

Hongwei Du, Hong Wang*

1 School of Materials Science and Engineering, Shanghai Jiao Tong University, Shanghai 200240, China.

2 Zhangjiang Institute for Advanced Study, Shanghai Jiao Tong University, Shanghai 201203, China.

3 Materials Genome Initiative Center, Shanghai Jiao Tong University, Shanghai 200240, China.

Abstract

Discovering new solid electrolytes (SEs) is essential to achieving higher safety and better energy density for all-solid-state lithium batteries. In this work, we introduce an advanced high-throughput virtual screening (HTVS) method that integrates the graph neural networks (GNN) for accurate property predictions. This approach ensures efficient and accurate predictions across various material properties, even with limited training data, by harnessing the power of transfer learning. Structure generation for promising candidates is achieved through the DiffCSP model, enabling precise crystal structure prediction. The pipeline is further refined by the application of DenseGNN for evaluating Li-ion conductivity, allowing for the selection of materials with optimal SE characteristics. The screening results in a few candidate materials, which are validated by density functional theory calculations and ab initio molecular dynamics simulations. The shortlisted oxysulfide materials satisfy key properties to be successful SEs. The advanced screening method presented in this work will accelerate the discovery of energy materials for related applications.

Introduction

Since Li-ion batteries (LiBs) have become prominent energy storage devices, a growing demand for batteries with safer and higher energy densities has led to the exploration of advanced technologies. All-solid-state battery (ASSB), which predominantly relies on solid electrolyte (SE)[1], demonstrates a promising potential as an advanced technology. SEs are anticipated to exceed the performance of current liquid electrolytes in LiBs in terms of three fundamental aspects of merit including energy density, safety, and cost. Despite their advantages, low ionic conductivities and limited stabilities impede their practical applications. Several types of SEs have been reported to date, including oxides, sulfides, and halides. Sulfide SEs, e.g., Li10GeP2S12 (LGPS), are characterized by their high ionic conductivity but poor stability, while oxide SEs, e.g., Li7La3Zr2O12 (LLZO), exhibited better chemical and electrochemical stability but lower ionic conductivity. It is thus desired to develop new SEs that achieve both high Li-ion conductivity and chemical/electrochemical stability. In order to develop improved SEs, oxysulfide materials were investigated to take advantage of the synergistic effect of sulfides and oxides, with the hope of discovering new SEs with both high stability and ionic conductivity[2, 3]. Additionally, the presence of halide elements was also expected to contribute to stability, as halide-type SEs are also known for their high stability similar to the oxide-type SEs[4].

High-throughput virtual screening (HTVS) is an efficient method to discover new materials from a large pool of candidates by evaluating various properties sequentially[5]. However, the current HTVS strategy has two significant challenges, a limited pool of materials and high computational cost of density functional theory (DFT) calculations[6-8]. Most HTVS begins with collecting materials from computational databases, such as Materials Project (MP)[9], which contains crystal structures and physical properties obtained from DFT calculations. Exploring the existing database, however, is unlikely to discover unreported materials with satisfying target properties due to the limited pool of materials. Thus, it is essential to expand the chemical space to explore. Structure generation approaches, such as elemental substitutions[10-12] or generative algorithms[13-15], could be used to overcome this limitation, although they could introduce another challenge in return, e.g., demanding computational resources to perform DFT calculations for structural relaxations and evaluation of other properties[16].

Instead of performing expensive DFT calculations for all candidate materials, deep learning (DL) models have been suggested to tackle this challenge. Using MP database as a training data, Crystal Graph Convolutional Neural Networks (CGCNN) [17]and MatErials Graph Network (MEGNet) [18] were developed, which achieved high accuracy for predicting formation energies. Despite their accuracies, they are not suitable for HTVS as they require relaxed structures to prepare input representations. Other approaches that require less or no information on geometries would be more appropriate for this purpose[19-21]. In this work, we expanded the chemical space, performed HTVS by applying different DL models to evaluate multiple properties, and identified several promising candidates for SEs.

To expand the chemical space, we initially generated hypothetical materials by performing elemental substitution on Li-containing materials. Subsequently, the thermodynamic stability, electronic conductivity, and electrochemical stability of the hypothetical materials were investigated by using a supervised DL model and a grand potential phase diagram, respectively. We then used an

supervised DL and generative models to select materials with high expected Li-ion conductivity based on their structures. Finally, we validated the selected candidate materials using DFT and ab initio molecular dynamics (AIMD) simulations.

Methods

Spin-polarized DFT calculations were performed using Vienna ab initio simulation package (VASP)[22] code with Perdew–Burke–Ernzerhof (PBE) exchange-correlation functional and the projector augmented wave (PAW) pseudopotentials[23]. All calculations were managed by an atomic simulation environment (ASE)[24]. The identical VASP parameters were chosen as in MP to compare thermodynamic and electronic properties of newly calculated materials with reference data deposited in MP (version: 2020.09.08). (11) This was done by setting "MaterialsProject2020Compatibility" tag in Pymatgen package[25]. In addition, the same version of the pseudopotentials was chosen for compatibility. For accurate bandgap calculations, the Heyd-Scuseria-Ernzerhof (HSE06) hybrid functional was employed[26, 27].

To predict lithium-ion conductivity, we conducted ab initio molecular dynamics (AIMD) simulations. The energies and forces along the trajectories were evaluated using non-spin-polarized density functional theory (DFT) calculations with a single Γ-centered k-point to expedite the computational process. All AIMD simulations were carried out within the NVT ensemble, employing a Nosé-Hoover thermostat and the Verlet algorithm to solve the equations of motion. During the AIMD simulations, the system was initially set to 100 K and then heated to the target temperatures (ranging from 600 to 1500 K) by velocity scaling over a period of 2 ps. The system was further equilibrated for 5 ps. To estimate the ionic conductivity at 300 K, a fitted relationship was used to extrapolate the results. Production runs were conducted for 40 ps at each temperature with a time step of 2 fs. The lithium-ion diffusivity (D) was determined from the mean squared displacement (MSD) over time. The ionic conductivity (σ) was calculated using the Nernst-Einstein relation. Conductivities were calculated using time intervals ranging from 10 to 40 ps of AIMD simulations, yielding multiple values to estimate a range of conductivity.

We employed Long Short-Term Memory and Gated Recurrent Unit fused with Deep Convolutional Neural Network(L-G-DCNN)[28], Representation Learning from Stoichiometry (Roost)[19] and compositionally restricted attention-based network (Crabnet)[29], an attention-based graph convolutional and transformer-based neural network for predicting materials properties using only stoichiometry as inputs. Notably, all models demonstrated superior performance compared to alternative ML models that rely on stoichiometry when trained on the MP database, which serves as our training data[30]. To train the models, we collected 96,357 sets of unique formula and their lowest formation energies among a total of 126,335 data deposited in MP. By utilizing an ensemble of 10 models, we achieved a mean absolute error (MAE) of 0.035 eV/atom for the test set of formation energy predictions (Figure S1a), which outperformed the accuracy of other composition-based models in prior studies[30]. To predict the synthesizability of materials, we calculate the crystal-likeness score (CLscore) of materials using positive and unlabeled DL (PU learning), as developed by Jang et al[31]., to quantify the probability of synthesis. We used a pretrained PU learning model that was trained on 124,515 unique crystal structure data queried from the MP database. Employing the DiffCSP[32] model, we conducted precise crystal structure

predictions for the shortlisted candidate materials. Subsequently, the well-trained DenseGNN[33] model was utilized to evaluate the Li-ion conductivity of the generated crystal structures, ensuring that the screened materials possess the potential to serve as solid electrolytes. Finally, the candidate materials were validated through Density Functional Theory (DFT) calculations and Ab Initio Molecular Dynamics (AIMD) simulations, confirming that their properties meet the key requirements for solid electrolytes.

Results

Chemical Space Expansion

To discover promising SEs that could outperform the state-of-the-art ones, it is essential to explore the chemical space beyond the existing database. We used the prototype structure-based elemental substitution method to broaden the chemical space[11]. Initially, 16,205 Li-containing ternary and quaternary materials were collected from MP, which were used as prototypes for the elemental substitution. We then determined promising elements in terms of market competitiveness, resulting in the selection of 28 elements (Li, B, C, N, O, F, Na, Mg, Al, Si, P, S, Cl, Ca, Zn, Ga, Ge, As, Se, Sr, Cd, In, Sn, Te, I, Ba, Hg, Pb). Some elements (H, Tc, and Pm) were not considered due to the lack of market competitiveness. We also note that all transition metals (TMs) were excluded since their byproducts can undergo redox reactions, as they can exist in various oxidation states[34]. In addition, the decomposed products containing TM elements generated by redox reactions are probable to be electronically conductive[35]. As sulfide-based SEs have demonstrated higher Li-ion conductivities compared to those of other types of electrolytes, we always included sulfur during the elemental substitution. In the case of $Li_xA_yB_z$, for example, all atomic positions were fixed, and the *A* and *B* were substituted with ones of the aforementioned 28 elements, while either *A* or *B* was set to sulfur. Thus, the elemental substitution of the example $Li_xA_yB_z$ resulted in 52 (= 26 × 2) structures. As a result of the elemental substitution, we generated a pool of 26,549,208 materials, which is approximately 1300 times larger than the MP database containing 16,205 ternary and quaternary materials in total. From this pool, we sequentially screened thermodynamic, electronic, and Li-ion conduction properties using various DL models in the following. The selected candidate materials were then validated by DFT and AIMD simulations. The overall screening procedure is schematically illustrated in Figure 1.

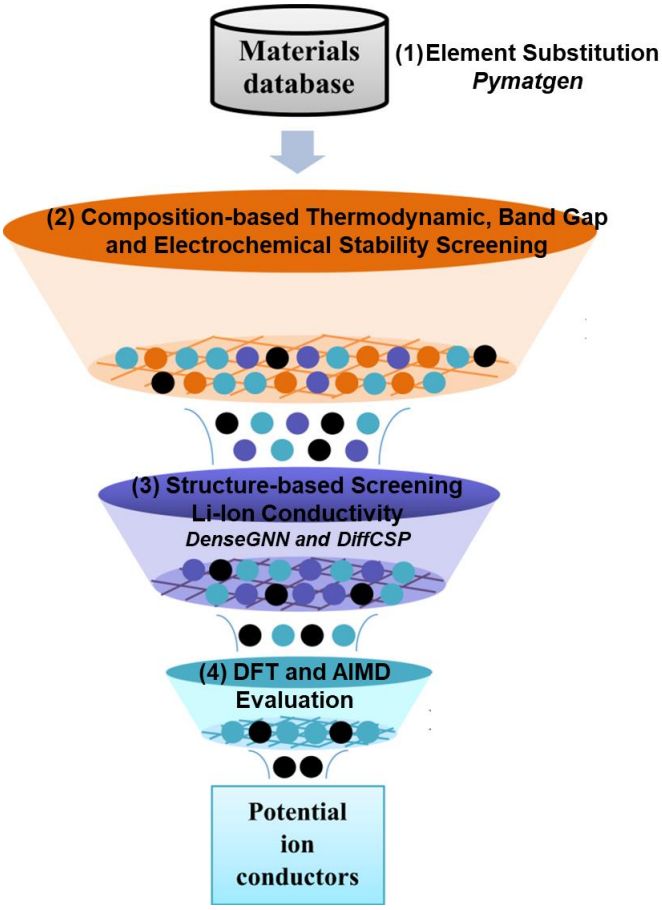

Figure 1. DL enabled the HTVS scheme consisting of four steps: (1) substitution structure generation, (2) composition-based screening of formation energies, energy above the hull, and electrochemical stability, (3) structure-based screening of Li-ion conductivity, and (4) validation of the selected candidate materials by DFT and AIMD simulations.

Composition-Based Screening: Thermodynamic Stability

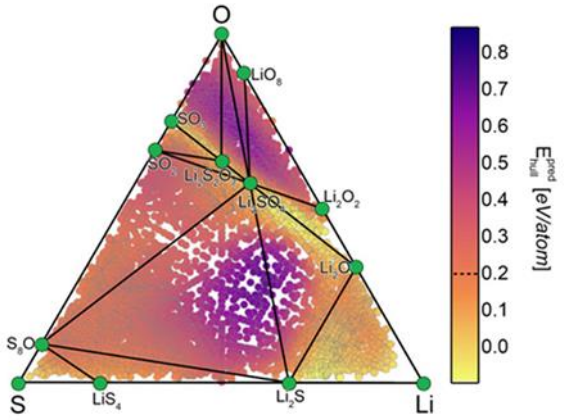

Figure 2. Energy above the convex hull (E_{hull}) plotted on the phase diagram of the Li–S–O system as an example. Green circles indicate the most stable ones (E_{hull} = 0 eV/atom) for the given compositions, while the rest correspond to materials with E_{hull} > 0 eV/atom.

We evaluated the thermodynamic stability of materials using two metrics: formation energy (E_f) and energy above the convex hull (E_{hull}). The formation energy is calculated to predict the thermodynamic stability, which is defined as the energy change that accompanies the formation of a substance from its constituent elements in their standard states[36]. For example, E_f of A_2B is calculated as $E_f = E_{A2B} - (2E_A + E_B)$, where E_{A2B} is the DFT energy of A_2B phase, and E_A and E_B are the DFT energies of A and B phases, respectively, in their most stable states as deposited in MP. Negative E_f indicates an exothermic formation process. In addition, the phase stability was evaluated by calculating E_{hull}, which is considered as a measure of the synthesizability of materials. E_{hull} is calculated as a vertical distance from the convex hull at the given composition in the Figure 2[37]. The previous work of Ceder et al. reported that the 90th percentile of synthesized inorganic materials in MP has E_{hull} of 0.067 eV/atom[38]. Thus, with some margin for exploration, we considered materials satisfying $E_f \leq 0$ and $E_{hull} \leq 0.1$ eV/atom as stable and synthesizable structures.

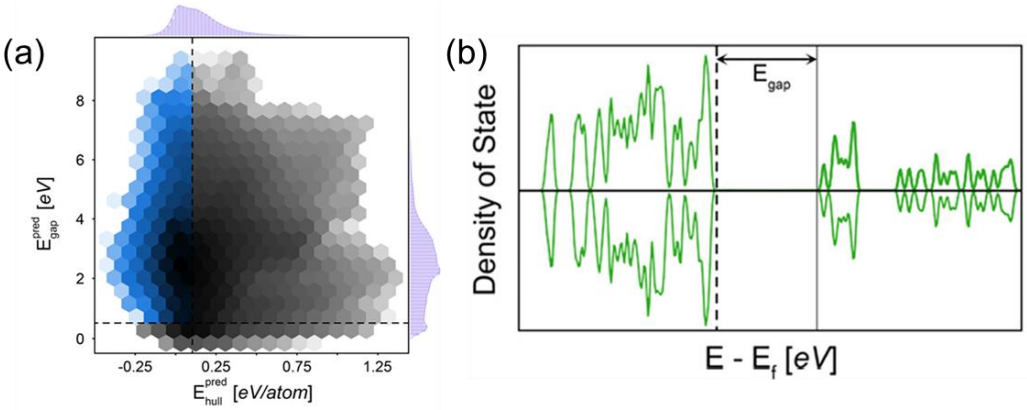

Figure 3. (a) Histogram of the predicted E_{hull} and E_{gap}. Dashed lines indicate the thresholds of each property. Blue symbols are selected for further analysis. (b) Density of states illustrating a band gap (E_{gap}) between the conduction and valence bands.

To properly evaluate the thermodynamics and phase stability of materials, geometry relaxations should be performed to obtain E_f and E_{hull}. Since it is computationally too demanding to calculate E_f and E_{hull} of 26,549,208 materials using DFT calculations, however, we instead took advantage of DL approaches. Representations of materials that do not require structure information are more suitable for this purpose, as the elemental substitution generated unrelaxed structures. We assumed that the predicted formation energy by Roost (E_f^{pred}) is that of the most stable structures for the given stoichiometry, i.e., $E_{hull} = 0$ eV/atom, since Roost cannot distinguish polymorphs. This means that the selected candidates require DFT validation at the end.

Figure 2, for example, shows the predicted energy above the convex hull (E_{hull}^{pred}) projected on the phase diagram of the Li–O–S system. Considering the uncertainty of the model, which was determined by the MAE of the ensemble method with 10 models, we determined chemical formulas satisfying both $E_f^{pred} \leq 0.1$ eV/atom and $E_{hull}^{pred} \leq 0.2$ eV/atom to be stable. Of 1,379,333, 954,301 chemical formulas satisfied these conditions (Figure 3a).

Composition-Based Screening: Electronic Conductivity

By the working mechanism of batteries, electrolyte materials must be ionically conductive but electronically insulating. Electrons passing through the electrolytes can cause self-discharge[39], Li dendrite growth[40], and consumption of component materials by side reactions, suggesting that the electronic conductivity of SEs should be minimized. Thus, we selected materials with bandgap (E_{gap}) larger than 1 eV to be suitable for this purpose (Figure 3b). This is the minimum acceptable value determined from the relationship between electrical conductivity and bandgap using crystalline silicon[34]. We highlight that this threshold was set to eliminate materials exhibiting electronic conductivity, and we also confirmed that tightening this threshold does not change the conclusion[34, 41]. Note that bandgap data in MP were calculated using the PBE functional, which is prone to underestimate bandgap with respect to experimental measurements[27]. Thus, the prediction DL model requires a more accurate data set to achieve high accuracy close to the experimental values. Since we only have 3896 experimental bandgap data[27], which are too few to develop an accurate DL model, we adopted a transfer learning approach[42], where we initially trained the Roost model using nonmetallic DFT-calculated 43,921 bandgap data taken from MP, followed by retraining the model using 3896 experimental data. This approach indeed helped to achieve higher prediction accuracy (MAE of 0.25 eV for the test set) using only a small number of training sets (Figure S1b). Using this trained model, we discarded compositions with the predicted bandgap smaller than 0.5 eV considering the test set MAE of the model, reducing the number of candidate chemical formulas from 954,301 to 797,557 (blue area in Figure 3a).

Composition-Based Screening: Electrochemical Stability

Another important factor required for promising SEs is a wide electrochemical stability window. The electrochemical stability window is a potential range within which SEs remain stable against electrochemical reactions. If the stability window of the SE is narrower than the operating potential range of the cell, interfacial layers restricting the migration of Li-ions can be formed on the electrode surfaces by decomposition of SEs[43]. Thus, it is desirable for SEs to have a wide electrochemical stability window to prevent their decomposition and maintain the long-term stability of the cell. To efficiently identify electrochemically stable SEs, we constructed grand potential phase diagrams that are in equilibrium with an open reservoir of Li[44]. This method identifies decomposition reactions of SEs at reductive and oxidative conditions and estimates potentials at which these reactions occur.

As a result, the decomposition energy diagram, which describes the stable potential region for SE, can be obtained, as shown in Figure 4a. While ϕ_{ox} obtained from this approach may overestimate practical values, it is still less than the formation energy-based method, thus effectively reducing the number of candidates during the screening process[34] (Supplementary Note 1).

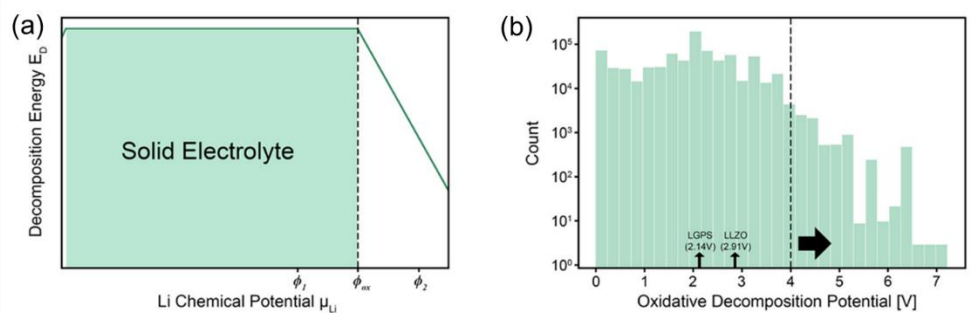

Figure 4. (a) Decomposition energy diagram as a function of the Li chemical potential (μ_{Li}). The SE is stable in a shaded potential range. (b) Histogram of oxidative decomposition potentials. The dashed line and arrow indicate the threshold of electrochemical stability and materials that satisfy this condition, respectively.

During the screening, we removed materials that are predicted to undergo oxidative decomposition reactions below 4 V[45, 46]. Similarly, SEs should remain stable below 0 V to utilize the high energy density of Li metal anodes, and this reductive decomposition could also be estimated by the same approach. However, all remaining candidates exhibited a reductive decomposition potential greater than 0 V, so the results could not be used for screening. Thus, we adopted only the oxidative decomposition potential for the current screening step. However, we note that the reductive decomposition potential was considered in the final step, where we ranked the electrochemical stability window ($\phi_{ox} - \phi_{red}$). Since the reductive decomposed products contain high Li content, it is probable that they will form passivation layers that are ionic conducive, and consequently, they can be less harmful compared to the oxidative products. For example, Li_3PS, Li_3PO_4, and LiPON form stable interfacial layers including different ionic conductors such as Li_3P, which protect SEs from the reductive decomposition[47-49]. The screening based on the oxidative decomposition potential resulted in 2138 compositions and 57,641 structures (Figure 4b). Afterward, we removed duplicated structures resulting in 14,535 structures (Figure S2).

Structure-Based Screening: Li-Ion Conductivity

An evaluation of Li-ion conductivity through DFT calculations, e.g., nudged elastic band (NEB) calculations and AIMD simulations, requires the optimized atomic structures and, thus, is computationally too intensive[50]. In this study, we constructed a platform consisting of a screening process and a GNN model to identify new superionic SEs candidates. The GNN model was constructed using a database consisting of the ionic conductivities and crystal system of various inorganic SEs, previously developed chemical descriptor[51], and the number of atoms. Using an ensemble of DenseGNN models, the prediction uncertainty was minimized. Each model performed 0.899, 0.923 ACCs, and 0.029, and 0.028 STDs, respectively. Through the screening process, 714 SEs candidates with potentially superior performance as SEs were derived from candidate Li-containing materials. To confirm the ionic conductivities of these candidates, the DFT and AIMD simulations were performed. Finally, three superionic SEs candidates that have not yet been investigated are proposed.

DFT Validations

For 714 candidate materials, we optimized their structures and assessed their structural characteristics, including space group and Wyckoff positions. This examination confirmed that none of these structures were present in the original MP database, ensuring that the screened structures are entirely novel. We calculated E_f and E_{hull}, where only 37 materials satisfied the thermodynamic stability conditions ($E_f < 0$ eV/atom and $E_{hull} < 0.1$ eV/atom) (Figure S4a). Furthermore, recognizing that thermodynamic properties, E_f and E_{hull}, alone do not fully assess synthesizability, we calculated the CLscore, a metric indicative of the synthesis probability, for the thermodynamically stable materials. Remarkably, 35 of these materials exhibited high synthesizability (CLscore > 0.5) (Figure S4b). We then evaluated their bandgap values using HSE06 functional, and all of them demonstrated higher bandgap than the threshold ($E_{gap} > 1$ eV). We also evaluated the electrochemical stability window for 35 candidates having 8 different compositions (Figure S5). By considering the electrochemical stability window, we chose 7 materials with the widest window, such as three polymorphs of Li_3ClSO_4, three polymorphs of Li_3FSO_4, and $Li_{10}C_4S_{16}$ (Figure S6). Followed by, their Li-ion conductivities were estimated from AIMD simulations.

The calculated band gap values and Li-ion conductivities are summarized in Figure 5, along with the electrochemical stability window and decomposition products. As a reference, we also evaluated Li-ion conductivity of LLZO, where our simulation results (0.28–6.18 mS/cm) covered the previously reported values (0.03–1.10 mS/cm)[52, 53]. We found that Li_3ClSO_4 and Li_3FSO_4, regardless of their structures, demonstrated better Li-ion conductivity than LLZO. Notably, all three polymorphs of Li_3ClSO_4 exhibited superior Li-ion conductivities (22.8, 26.0, and 30.8 mS/cm on average) compared to LGPS (12 mS/cm), which is widely regarded as one of the best solid Li-ion conductors[54].

formula	prototype structure (MPID)	type	reductive decomposition product	electrochemical stability range [V]	oxidative decomposition product	E_{hull} [eV/atom]	CLscore	E_{gap} [eV]	ionic conductivity range at 300 K [mS/cm]
Li_3ClSO_4	mp-559106	α	Li_2S, Li_2O, LiCl	1.57–4.27	Li_2SO_4, Cl_2	0.024	0.817	7.4	17.12–28.51
	mp-18002	β				0.050	0.810	7.2	25.82–35.81
	mp-559904	γ				0.073	0.736	6.6	12.98–39.06
Li_3FSO_4	mp-559106	α	Li_2S, Li_2O, LiF	1.57–4.58	$LiSO_3F$, O_2	0.038	0.842	7.8	1.30–4.69
	mp-18002	β				0.053	0.690	7.2	7.88–10.21
	mp-559904	γ				0.075	0.598	7.3	5.38–16.94
$Li_{10}C_4SO_{16}$	mp-1147687		Li_2S, Li_2O, Li_2CO_3	1.57–4.09	Li_2SO_4, CO_2, O_2	0.041	0.713	7.2	0.23–1.05
$Li_7La_3Zr_2O_{12}$(LLZO)	mp-942733		Zr_3O, Li_2O, La_2O_3	0.05–2.91	$Li_6Zr_2O_7$, Li_2O_2, La_2O_3	0.000	0.641	5.6 (5.8) (67)	0.28–6.18 (0.03–1.10) (62,63,68)
$Li_{10}GeP_2S_{12}$(LGPS)	mp-696128		Li_4GeS_4, P, Li_2S	1.71–2.14	Li_3PS_4, S, GeS_2	0.030	0.141	(3.6) (48)	(12.00) (64)

Figure 5. DFT-Calculated Properties of 7 Selected Phases

Discussion

In this work, we proposed the DL-assisted HTVS method to explore undiscovered chemical space. This method enabled efficient material exploration by significantly reducing the computational cost compared to conventional DFT-based HTVS. Approximately 27 million candidates generated by the elemental substitution method were subsequently narrowed down to a manageable quantity for DFT-level simulations. These structures were then validated by DFT and AIMD simulations, and new candidates for SEs with improved properties were proposed. These suggested materials were predicted to exhibit Li-ion conductivity as high as sulfide-type SEs while also achieving a wide electrochemical stability window similar to oxide-type SEs.

To further improve the HTVS method in future studies, we discuss two aspects in the following: the HTVS method and chemical space exploration. In HTVS, we highlight that the order of screening procedures was determined to minimize the computational cost. The results would remain the same even if the screening were performed in a different order, but it would come at the cost of increased computational resources and a longer processing time, suggesting the importance of efficient HTVS structure. Second, a more accurate DL method for stability prediction should be developed. DFT validations demonstrated that only 5% of the structures were indeed calculated to be stable, although all of them were predicted to be stable by DL (Figure S4). This is due to the limitations of using stoichiometric information as sole input representations, which does not account for the impact of bond structures on the stability. Third, in pursuit of the objective of our work, we overlooked several properties that may play crucial roles in the development of SEs for LiBs, including the ionic conduction property of the reductively decomposed products of SEs.

The success of the materials discovery is heavily dependent on the quality and diversity of the initial data set used, which could be improved by incorporating more advanced structure generation methods compared to the current substitution method. As a part of the future work, we plan to integrate generative models such as genetic algorithms (GAs)[55] and generative adversarial networks (GANs)[15]. By combining these methods with our DL-assisted HTVS approach, we aim to mitigate the weaknesses of the current method for the discovery of advanced materials.

AUTHOR INFORMATION

Corresponding Authors

Hong Wang - *School of Materials Science and Engineering, Shanghai Jiao Tong University, Shanghai 200240, China;* Email: hongwang2@sjtu.edu.cn

Authors

Hongwei Du - *School of Materials Science and Engineering, Shanghai Jiao Tong University, Shanghai 200240, China*

Author Contributions

Hongwei Du, and Hong Wang devised the idea for the paper. Hongwei Du implemented the idea and conducted the code design and visualizations. Hongwei Du and Hong Wang interpreted the results and prepared the manuscript.

Notes

The authors declare no competing financial interest.

ASSOCIATED CONTENT

Supporting Information

Performances of DL models, removal procedure of duplicated structures, procedure of structure generation, DFT and AIMD validation results.

ACKNOWLEDGMENTS

We are grateful for the financial support from the National Key Research and Development Program of China (Grant Nos.2021YFB3702102). The computations in this paper were run on the π 2.0 cluster supported by the Center for High Performance Computing at Shanghai Jiao Tong University.

REFERENCES

(1) Weppner, W. Engineering of solid state ionic devices. *Ionics* **2003**, *9* (5), 444-464. DOI: 10.1007/BF02376599.

(2) Kim, K.-H.; Martin, S. W. Structures and Properties of Oxygen-Substituted Li10SiP2S12–xOx Solid-State Electrolytes. *Chemistry of Materials* **2019**, *31* (11), 3984-3991. DOI: 10.1021/acs.chemmater.9b00505.

(3) Wang, X.; Xiao, R.; Li, H.; Chen, L. Oxysulfide LiAlSO: A Lithium Superionic Conductor from First Principles. *Physical Review Letters* **2017**, *118* (19), 195901. DOI: 10.1103/PhysRevLett.118.195901.

(4) Wang, C.; Liang, J.; Kim, J. T.; Sun, X. Prospects of halide-based all-solid-state batteries: From material design to practical application. *Science Advances 8* (36), eadc9516. DOI: 10.1126/sciadv.adc9516 (acccessed 2024/08/09).

(5) Pyzer-Knapp, E. O.; Suh, C.; Gómez-Bombarelli, R.; Aguilera-Iparraguirre, J.; Aspuru-Guzik, A. What Is High-Throughput Virtual Screening? A Perspective from Organic Materials Discovery. *Annual Review of Materials Research* **2015**, *45* (Volume 45, 2015), 195-216. DOI: https://doi.org/10.1146/annurev-matsci-070214-020823.

(6) Xiao, Y.; Miara, L. J.; Wang, Y.; Ceder, G. Computational Screening of Cathode Coatings for Solid-State Batteries. *Joule* **2019**, *3* (5), 1252-1275. DOI: https://doi.org/10.1016/j.joule.2019.02.006.

(7) Aykol, M.; Kim, S.; Hegde, V. I.; Snydacker, D.; Lu, Z.; Hao, S.; Kirklin, S.; Morgan, D.; Wolverton, C. High-throughput computational design of cathode coatings for Li-ion batteries. *Nature Communications* **2016**, *7* (1), 13779. DOI: 10.1038/ncomms13779.

(8) Honrao, S. J.; Yang, X.; Radhakrishnan, B.; Kuwata, S.; Komatsu, H.; Ohma, A.; Sierhuis, M.; Lawson, J. W. Discovery of novel Li SSE and anode coatings using interpretable machine learning and high-throughput multi-property screening. *Scientific Reports* **2021**, *11* (1), 16484. DOI: 10.1038/s41598-021-94275-5.

(9) Jain, A.; Ong, S. P.; Hautier, G.; Chen, W.; Richards, W. D.; Dacek, S.; Cholia, S.; Gunter, D.; Skinner, D.; Ceder, G.; et al. Commentary: The Materials Project: A materials genome approach to accelerating materials innovation. *APL Materials* **2013**, *1* (1), 011002. DOI: 10.1063/1.4812323 (acccessed 8/9/2024).

(10) Hautier, G.; Fischer, C.; Ehrlacher, V.; Jain, A.; Ceder, G. Data Mined Ionic Substitutions for the Discovery of New Compounds. *Inorganic Chemistry* **2011**, *50* (2), 656-663. DOI: 10.1021/ic102031h.

(11) Wang, H.-C.; Botti, S.; Marques, M. A. L. Predicting stable crystalline compounds using chemical similarity. *npj Computational Materials* **2021**, *7* (1), 12. DOI: 10.1038/s41524-020-00481-6.

(12) Kusaba, M.; Liu, C.; Yoshida, R. Crystal structure prediction with machine learning-based element substitution. *Computational Materials Science* **2022**, *211*, 111496. DOI: https://doi.org/10.1016/j.commatsci.2022.111496.

(13) Wang, Y.; Lv, J.; Zhu, L.; Ma, Y. CALYPSO: A method for crystal structure prediction. *Computer Physics Communications* **2012**, *183* (10), 2063-2070. DOI: https://doi.org/10.1016/j.cpc.2012.05.008.

(14) Court, C. J.; Yildirim, B.; Jain, A.; Cole, J. M. 3-D Inorganic Crystal Structure Generation and Property Prediction via Representation Learning. *Journal of Chemical Information and Modeling* **2020**, *60* (10), 4518-4535. DOI: 10.1021/acs.jcim.0c00464.

(15) Long, T.; Fortunato, N. M.; Opahle, I.; Zhang, Y.; Samathrakis, I.; Shen, C.; Gutfleisch, O.; Zhang, H. Constrained crystals deep convolutional generative adversarial network for the inverse design of crystal structures. *npj Computational Materials* **2021**, *7* (1), 66. DOI: 10.1038/s41524-021-00526-4.

(16) He, B.; Chi, S.; Ye, A.; Mi, P.; Zhang, L.; Pu, B.; Zou, Z.; Ran, Y.; Zhao, Q.; Wang, D.; et al. High-throughput screening platform for solid electrolytes combining hierarchical ion-transport prediction algorithms. *Scientific Data* **2020**, *7* (1), 151. DOI: 10.1038/s41597-020-0474-y.
(17) Xie, T.; Grossman, J. C. Crystal Graph Convolutional Neural Networks for an Accurate and Interpretable Prediction of Material Properties. *Physical Review Letters* **2018**, *120* (14), 145301. DOI: 10.1103/PhysRevLett.120.145301.
(18) Chen, C.; Ye, W.; Zuo, Y.; Zheng, C.; Ong, S. P. Graph Networks as a Universal Machine Learning Framework for Molecules and Crystals. *Chemistry of Materials* **2019**, *31* (9), 3564-3572. DOI: 10.1021/acs.chemmater.9b01294.
(19) Goodall, R. E. A.; Lee, A. A. Predicting materials properties without crystal structure: deep representation learning from stoichiometry. *Nature Communications* **2020**, *11* (1), 6280. DOI: 10.1038/s41467-020-19964-7.
(20) Mok, D. H.; Shin, D.; Na, J.; Back, S. A chemically inspired convolutional neural network using electronic structure representation. *Journal of Materials Chemistry A* **2023**, *11* (19), 10184-10194, 10.1039/D3TA01767B. DOI: 10.1039/D3TA01767B.
(21) Mok, D. H.; Kim, J.; Back, S. Direction-Based Graph Representation to Accelerate Stable Catalyst Discovery. *Chemistry of Materials* **2022**, *35* (1), 63-70. DOI: 10.1021/acs.chemmater.2c02498.
(22) Kresse, G.; Hafner, J. Ab initio molecular dynamics for liquid metals. *Physical Review B* **1993**, *47* (1), 558-561. DOI: 10.1103/PhysRevB.47.558.
(23) Blöchl, P. E. Projector augmented-wave method. *Physical Review B* **1994**, *50* (24), 17953-17979. DOI: 10.1103/PhysRevB.50.17953.
(24) Hjorth Larsen, A.; Jørgen Mortensen, J.; Blomqvist, J.; Castelli, I. E.; Christensen, R.; Dułak, M.; Friis, J.; Groves, M. N.; Hammer, B.; Hargus, C.; et al. The atomic simulation environment—a Python library for working with atoms. *Journal of Physics: Condensed Matter* **2017**, *29* (27), 273002. DOI: 10.1088/1361-648X/aa680e.
(25) Ong, S. P.; Richards, W. D.; Jain, A.; Hautier, G.; Kocher, M.; Cholia, S.; Gunter, D.; Chevrier, V. L.; Persson, K. A.; Ceder, G. Python Materials Genomics (pymatgen): A robust, open-source python library for materials analysis. *Computational Materials Science* **2013**, *68*, 314-319. DOI: https://doi.org/10.1016/j.commatsci.2012.10.028.
(26) Heyd, J.; Scuseria, G. E.; Ernzerhof, M. Erratum: “Hybrid functionals based on a screened Coulomb potential” [J. Chem. Phys. 118, 8207 (2003)]. *The Journal of Chemical Physics* **2006**, *124* (21), 219906. DOI: 10.1063/1.2204597 (acccessed 8/9/2024).
(27) Zhuo, Y.; Mansouri Tehrani, A.; Brgoch, J. Predicting the Band Gaps of Inorganic Solids by Machine Learning. *The Journal of Physical Chemistry Letters* **2018**, *9* (7), 1668-1673. DOI: 10.1021/acs.jpclett.8b00124.
(28) Du, H.; Hui, J.; Zhang, L.; Wang, H. Rational Design of Deep Learning Networks Based on a Fusion Strategy for Improved Material Property Predictions. *Journal of Chemical Theory and Computation* **2024**. DOI: 10.1021/acs.jctc.4c00187.
(29) Wang, A. Y.-T.; Kauwe, S. K.; Murdock, R. J.; Sparks, T. D. Compositionally restricted attention-based network for materials property predictions. *npj Computational Materials* **2021**, *7* (1), 77. DOI: 10.1038/s41524-021-00545-1.
(30) Bartel, C. J.; Trewartha, A.; Wang, Q.; Dunn, A.; Jain, A.; Ceder, G. A critical examination of compound stability predictions from machine-learned formation energies. *npj Computational Materials* **2020**, *6* (1), 97. DOI: 10.1038/s41524-020-00362-y.

(31) Jang, J.; Gu, G. H.; Noh, J.; Kim, J.; Jung, Y. Structure-Based Synthesizability Prediction of Crystals Using Partially Supervised Learning. *Journal of the American Chemical Society* **2020**, *142* (44), 18836-18843. DOI: 10.1021/jacs.0c07384.
(32) <Crystal Structure Prediction.pdf>.
(33) Wang, H.; Du, H.; Hui, J.; zhang, l. **2024**. DOI: 10.21203/rs.3.rs-4173966/v1.
(34) Sendek, A. D.; Yang, Q.; Cubuk, E. D.; Duerloo, K.-A. N.; Cui, Y.; Reed, E. J. Holistic computational structure screening of more than 12 000 candidates for solid lithium-ion conductor materials. *Energy & Environmental Science* **2017**, *10* (1), 306-320, 10.1039/C6EE02697D. DOI: 10.1039/C6EE02697D.
(35) Xiao, Z.; Yan, L.; Hu, Q.; Xiang, B.; Wang, Y.; Hao, J.; Zou, X.; Li, W.; Wei, S. Doping-driven electronic structure and conductivity modification of nickel sulfide. *Dalton Transactions* **2022**, *51* (21), 8318-8326, 10.1039/D2DT00363E. DOI: 10.1039/D2DT00363E.
(36) Agrawal, A.; Meredig, B.; Wolverton, C.; Choudhary, A. A Formation Energy Predictor for Crystalline Materials Using Ensemble Data Mining. In *2016 IEEE 16th International Conference on Data Mining Workshops (ICDMW)*, 12-15 Dec. 2016, 2016; pp 1276-1279. DOI: 10.1109/ICDMW.2016.0183.
(37) Barber, C. B.; Dobkin, D. P.; Huhdanpaa, H. The quickhull algorithm for convex hulls. *ACM Trans. Math. Softw.* **1996**, *22* (4), 469–483. DOI: 10.1145/235815.235821.
(38) Sun, W.; Dacek, S. T.; Ong, S. P.; Hautier, G.; Jain, A.; Richards, W. D.; Gamst, A. C.; Persson, K. A.; Ceder, G. The thermodynamic scale of inorganic crystalline metastability. *Science Advances 2* (11), e1600225. DOI: 10.1126/sciadv.1600225 (acccessed 2024/08/09).
(39) Lotsch, B. V.; Maier, J. Relevance of solid electrolytes for lithium-based batteries: A realistic view. *Journal of Electroceramics* **2017**, *38* (2), 128-141. DOI: 10.1007/s10832-017-0091-0.
(40) Han, F.; Westover, A. S.; Yue, J.; Fan, X.; Wang, F.; Chi, M.; Leonard, D. N.; Dudney, N. J.; Wang, H.; Wang, C. High electronic conductivity as the origin of lithium dendrite formation within solid electrolytes. *Nature Energy* **2019**, *4* (3), 187-196. DOI: 10.1038/s41560-018-0312-z.
(41) Muy, S.; Voss, J.; Schlem, R.; Koerver, R.; Sedlmaier, S. J.; Maglia, F.; Lamp, P.; Zeier, W. G.; Shao-Horn, Y. High-Throughput Screening of Solid-State Li-Ion Conductors Using Lattice-Dynamics Descriptors. *iScience* **2019**, *16*, 270-282. DOI: https://doi.org/10.1016/j.isci.2019.05.036.
(42) Tan, C.; Sun, F.; Kong, T.; Zhang, W.; Yang, C.; Liu, C. A Survey on Deep Transfer Learning. In *Artificial Neural Networks and Machine Learning – ICANN 2018*, Cham, 2018//, 2018; Kůrková, V., Manolopoulos, Y., Hammer, B., Iliadis, L., Maglogiannis, I., Eds.; Springer International Publishing: pp 270-279.
(43) Lu, Z.; Ciucci, F. Metal Borohydrides as Electrolytes for Solid-State Li, Na, Mg, and Ca Batteries: A First-Principles Study. *Chemistry of Materials* **2017**, *29* (21), 9308-9319. DOI: 10.1021/acs.chemmater.7b03284.
(44) Mo, Y.; Ong, S. P.; Ceder, G. First Principles Study of the Li10GeP2S12 Lithium Super Ionic Conductor Material. *Chemistry of Materials* **2012**, *24* (1), 15-17. DOI: 10.1021/cm203303y.
(45) Manthiram, A. A reflection on lithium-ion battery cathode chemistry. *Nature Communications* **2020**, *11* (1), 1550. DOI: 10.1038/s41467-020-15355-0.
(46) Manthiram, A. An Outlook on Lithium Ion Battery Technology. *ACS Central Science* **2017**, *3* (10), 1063-1069. DOI: 10.1021/acscentsci.7b00288.
(47) Liu, Z.; Fu, W.; Payzant, E. A.; Yu, X.; Wu, Z.; Dudney, N. J.; Kiggans, J.; Hong, K.; Rondinone, A. J.; Liang, C. Anomalous High Ionic Conductivity of Nanoporous β-Li3PS4. *Journal of the American Chemical Society* **2013**, *135* (3), 975-978. DOI: 10.1021/ja3110895.

(48) Nazri, G. Preparation, structure and ionic conductivity of lithium phosphide. *Solid State Ionics* **1989**, *34* (1), 97-102. DOI: https://doi.org/10.1016/0167-2738(89)90438-4.

(49) Richards, W. D.; Miara, L. J.; Wang, Y.; Kim, J. C.; Ceder, G. Interface Stability in Solid-State Batteries. *Chemistry of Materials* **2016**, *28* (1), 266-273. DOI: 10.1021/acs.chemmater.5b04082.

(50) Car, R.; Parrinello, M. Unified Approach for Molecular Dynamics and Density-Functional Theory. *Physical Review Letters* **1985**, *55* (22), 2471-2474. DOI: 10.1103/PhysRevLett.55.2471.

(51) Ward, L.; Agrawal, A.; Choudhary, A.; Wolverton, C. A general-purpose machine learning framework for predicting properties of inorganic materials. *npj Computational Materials* **2016**, *2* (1), 16028. DOI: 10.1038/npjcompumats.2016.28.

(52) He, X.; Zhu, Y.; Epstein, A.; Mo, Y. Statistical variances of diffusional properties from ab initio molecular dynamics simulations. *npj Computational Materials* **2018**, *4* (1), 18. DOI: 10.1038/s41524-018-0074-y.

(53) Li, Y.; Han, J.-T.; Wang, C.-A.; Vogel, S. C.; Xie, H.; Xu, M.; Goodenough, J. B. Ionic distribution and conductivity in lithium garnet Li7La3Zr2O12. *Journal of Power Sources* **2012**, *209*, 278-281. DOI: https://doi.org/10.1016/j.jpowsour.2012.02.100.

(54) Kamaya, N.; Homma, K.; Yamakawa, Y.; Hirayama, M.; Kanno, R.; Yonemura, M.; Kamiyama, T.; Kato, Y.; Hama, S.; Kawamoto, K.; et al. A lithium superionic conductor. *Nature Materials* **2011**, *10* (9), 682-686. DOI: 10.1038/nmat3066.

(55) Glass, C. W.; Oganov, A. R.; Hansen, N. USPEX—Evolutionary crystal structure prediction. *Computer Physics Communications* **2006**, *175* (11), 713-720. DOI: https://doi.org/10.1016/j.cpc.2006.07.020.